# Supporting Information

Venkateshwaran et al. 10.1073/pnas.1403294111

## SI Text

**Sensitivity of the Potential of Mean Force Between Oppositely Charged Ions to Locations on the Liquid Side of the Interface.** Fig. S1 shows a close-up view of potential of mean force (PMF) profiles between an oppositely charged ion pair at various $z$ locations on the liquid side of the interface. In the subsurface layers, the effective ion–ion interaction is strengthened by 3–10 kJ/mol, depending on the exact location of the ion pair relative to the interface. Ionic groups of surfactants or proteins are likely to be located in this region when these molecules are present at the interface. Fig. S1 shows that even in the subsurface layers, the enhancement of effective ion–ion interactions is likely strong enough to affect biological structure and stability at the interface.

**Comparison Between Particle Mesh Ewald and Slab Ewald Calculations.** The results presented in Figs. 1 and 2 in the main text are obtained from simulations using the standard particle mesh Ewald (PME) treatment of electrostatic interactions. We performed additional simulations using the slab Ewald method (1), which accounts for the slab geometry of the system more faithfully and has been shown to produce results in quantitative agreement with rigorous 2D Ewald calculations (1). Fig. S2 shows a comparison of the $W(r|z)$ profiles for a $M^+ - M^-$ ion pair at three different $z$ locations, calculated using the standard PME and the slab Ewald method. The agreement between the two is excellent.

**The System Size Dependence of PMFs.** Because different factors contribute to different extents to the ion–ion PMF, depending on the location of the ion pair relative to the interface, obtaining a quantitative understanding of the system size dependence of the ion–ion PMF is a challenging task. In bulk water, correctly accounting for image interactions (i.e., performing the Ewald calculation correctly) (2) provides system size-independent ion–ion PMF. At the interface, however, capillary correlations and interface deformation (on the vapor side) contribute to the ion–ion PMF, and their system size dependence can be nontrivial. Fig. S3 shows the $W(r|z)$ profiles for the $M^+ - M^-$ ion pair at various $z$ locations, obtained from simulations with a box having a 7.0-nm × 7.0-nm cross section, i.e., a four times larger box cross section than that used in Fig. 1 in the main text. The PMF profiles from the larger system show trends similar to that for the smaller box. For example, there is a sharp decrease in the contact minimum as the ion pair is drawn to the vapor side of the interface. At the interface and on the vapor side, the $W(r|z)$ profile shows a long-ranged tail.

A direct numerical comparison of the PMF profiles at various $z$ locations on the vapor side of the interface obtained from the smaller and larger boxes is shown in Fig. S4. To enable comparison, we have set PMFs to zero at the contact minimum configuration ($r = 0.39$ nm) in Fig. S4. Although the trends are similar, how do we reconcile the differences between the two? At $z = 0$, interface deformation plays a negligible role in the ion–ion PMF and long-range correlations arise from capillary waves (3–5). Indeed, the long-range parts of the ion–ion correlation, $g(r|z=0) = \exp(-W(r|z=0)/k_BT)$, from different box lengths are related to each other by a simple scaling of the $r$ dimension by the box length $L$, $\tilde{r} = r/L$ (Fig. S5).

As the ion pair is moved to the vapor side, in addition to the capillary correlations, interface deformation (its system size dependence and its effect on the capillary correlation) adds to the long-range nature of $W(r|z)$ in a nontrivial manner. To compare $W(r|z)$ profiles from different systems, in addition to ion separation, the extent of deformation (i.e., $z$) may need to be scaled. In other words, for larger systems, interface deformation may need to be proportionally larger. Indeed, effective attraction between larger millimeter-sized colloidal particles arising from interface deformation is well known (6, 7).

**Charge Density Dependence of the PMF Between Oppositely Charged Ions.** Ion charge density influences not only the free energy of moving a single ion in the $z$ direction (e.g., the presence/absence of the free energy minimum near the interface) but also the effective ion–ion interaction at the interface (Fig. S6). We expect both the ion hydration and capillary pinning contributions to be larger for ion pairs of higher charge density based on results in the main text. Indeed, we find that enhancement of the effective ion–ion attractions is higher for charge pairs with higher charge densities.

**PMF Between the Peptide Ends in Bulk Water.** Fig. S7 shows the PMFs between the $C_\alpha$ ends of the end-charged and neutral versions of the peptide in bulk water and at the interface calculated using umbrella sampling simulations. The neutral peptide displays similar structural preferences in bulk water and at the interface, forming a single α-helical turn configuration. In contrast, the charged ends of $^+GL_5G^-$ peptide are well hydrated and prefer to be separated from each other in bulk water, but form a stable contact in the subsurface interfacial region, leading to a hairpin-turn–like conformation.


1. Yeh IC, Berkowitz ML (1999) Ewald summation for systems with slab geometry. *J Chem Phys* 111:3155–3162.
2. Hummer G, Pratt LR, García AE (1996) Free energy of ionic hydration. *J Phys Chem* 100(4):1206–1215.
3. Buff F, Lovett R, Stillinger F (1965) Interfacial density profile for fluids in the critical region. *Phys Rev Lett* 15(15):621–624.
4. Rowlinson JS, Widom B (2002) *Molecular Theory of Capillarity* (Dover, Mineola, NY).
5. Weeks JD (1977) Structure and thermodynamics of the liquid–vapor interface. *J Chem Phys* 67:3106–3121.
6. Stamou D, Duschl C, Johannsmann D (2000) Long-range attraction between colloidal spheres at the air-water interface: The consequence of an irregular meniscus. *Phys Rev E Stat Phys Plasmas Fluids Relat Interdiscip Topics* 62(4 Pt B):5263–5272.
7. Nikolaides MG, et al. (2002) Electric-field-induced capillary attraction between like-charged particles at liquid interfaces. *Nature* 420(6913):299–301.

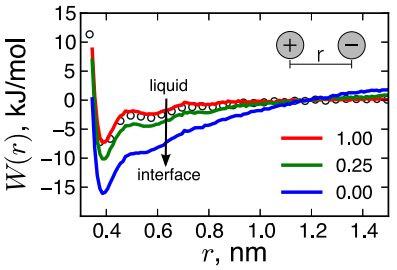


**Fig. S1.** PMF profiles for the $M^+ - M^-$ ion pair at various $z$ locations on the liquid side of the interface. The ion–ion PMF in bulk water is also shown for reference (open circles).

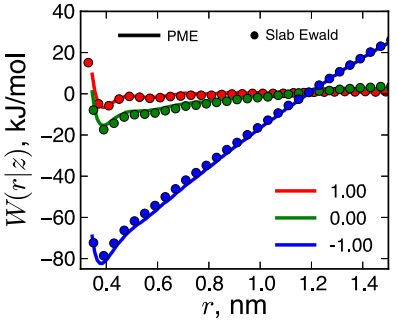


**Fig. S2.** Comparison of PMF profiles at three different $z$ locations for the $M^+ - M^-$ ion pair computed from simulations using the particle mesh Ewald method in three dimensions (–) and the slab Ewald method (•) (1) for treating electrostatic interactions.

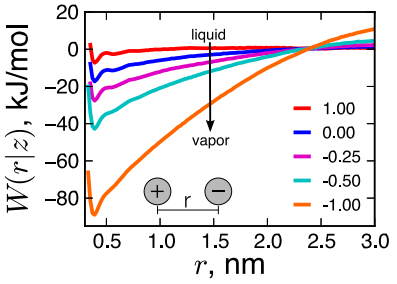


**Fig. S3.** PMF profiles for the $M^+ - M^-$ ion pair computed in a box with $xy$ cross section of 7.0 nm × 7.0 nm at various $z$ locations. The PMF profiles have been set to zero at $r = 2.4$ nm for reference.

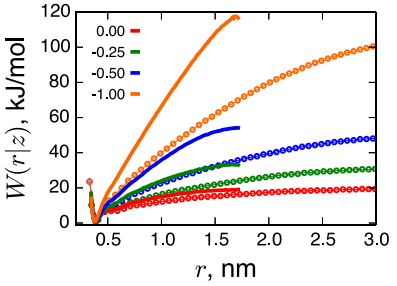


**Fig. S4.** Comparison of PMF profiles for the $M^+ - M^-$ ion pair computed in two different boxes with $xy$ cross section of 7.0 nm × 7.0 nm and 3.5 nm × 3.5 nm for $z$ locations on the vapor side of the interface ($z \leq 0$).

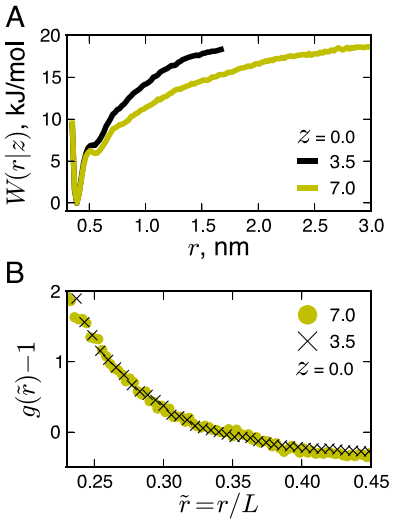


**Fig. S5.** (*A*) Comparison of PMF profiles for the $M^+ - M^-$ ion pair computed in two different boxes with *xy* cross section of 7.0 nm × 7.0 nm and 3.5 nm × 3.5 nm at $z = 0.0$. The PMF profiles have been set to zero at the contact distance of $r = 0.39$ nm. These are the same PMFs as in Fig. S4 for $z = 0$. (*B*) $g(\tilde{r}) - 1$ for $z = 0.0$ plotted as a function of the dimensionless distance $\tilde{r} = r/L$ for two different box lengths, $L = 7.0$ nm (•) and $L = 3.5$ nm (X).

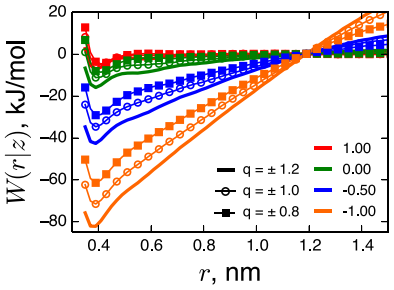


**Fig. S6.** PMFs for oppositely charged ions calculated at four different *z* locations. PMFs are shown for three different values of charges on the ions, $q = \pm 0.8e$, $\pm 1.0e$, and $\pm 1.2e$.

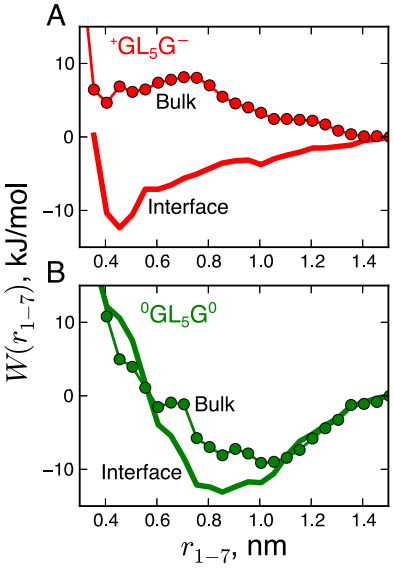


**Fig. S7.** (*A* and *B*) Comparison of the peptide end-to-end PMF profiles in bulk water and at the interface for (*A*) end-charged $^{+}GL_5G^{-}$ and (*B*) neutral $^{0}GL_5G^{0}$ peptides calculated using umbrella sampling simulations.